NUMERICAL INVESTIGATION OF THE ROTOR-ROTOR AERODYNAMIC INTERACTION OF eVTOL CONFIGURATIONS BY A MID-FIDELITY APPROACH

Alex Zanotti*, Riccardo Piccinini, Matteo Tugnoli
Politecnico di Milano, Milano — Italy
* alex.zanotti@polimi.it

Abstract
The rotor-rotor aerodynamic interaction is one of the characteristic phenomena that influence both flow physics and performance of most of the new electric vehicles for urban air mobility (eVTOLs) widely investigated in recent years. The present article describes a numerical activity aimed to the systematic study of the rotor-rotor aerodynamic interaction with application to eVTOLs cruise flight condition. The activity considers numerical simulations performed with DUST, a novel mid-fidelity aerodynamic solver based on vortex particle method. In particular, the test case considered consists of two propellers both in side-by-side and tandem configuration. Simulations results highlighted quantitatively the loss of propellers performance by varying separations distance between them and provided a detailed insight about flow physics involved in such aerodynamic interactions.

1 INTRODUCTION

A great interest and development effort has been devoted in recent years towards design of unconventional VTOL aircraft based on electric distributed propulsion (eVTOLs) aimed to create a novel concept of urban air mobility (UAM) [1]. Most of eVTOLs architectures are characterised by the use of multi-propellers configurations, thus, from aerodynamic point of view, the rotor-rotor interaction represents one of the key phenomena that influences eVTOLs flow field as well as their performance, handling qualities, and noise impact. Looking at typical architectures of eVTOL aircraft (see Fig. 1), two main types of rotor-rotor aerodynamic interaction can be outlined as the more interesting, i.e. with propellers in side-by-side and tandem configurations. These kinds of aerodynamic interaction have been investigated in recent literature both in experimental and numerical field with main focus on applications of small drones in hover, e.g. [2, 3, 4, 5]. Despite these studies, there is a certain lack in literature of a systematic study on these aerodynamic interactions for eVTOLs aircraft applications, particularly in cruise flight condition. The present work was therefore aimed to perform a numerical parametric study of the aerodynamic interaction between two propellers both in side-by-side and tandem configuration. Simulations consider different longitudinal distances and several degrees of overlapping between propellers disks. In particular, the present numerical activity was focused on propellers advance ratio corresponding to the target cruise condition of a eVTOL aircraft in urban areas. Numerical simulations were performed using the mid-fidelity aerodynamic open-source software DUST developed by Politecnico di Milano [6, 7].

(a) Vahana by A^3 by Airbus LLC

(b) Bell-Nexus 6HX

Figure 1: Examples of eVTOLs aircraft architectures: (**a**) Vahana by A^3 by Airbus LLC, (**b**) Bell-Nexus 6HX by Bell

This code, based on the use of vortex particle method

Presented at the 47th European Rotorcraft Forum, Glasgow, UK, 7-10 September, 2021

(VPM) [8] for wake modelling, was thoroughly validated against experiments and high fidelity CFD on different rotorcraft configurations, from simpler rotor-wing test cases [7] to the full XV-15 tiltrotor [9] and Vahana eVTOL vehicle [10]. The complete mathematical formulation of the solver was described in [7]. Thanks to the low computational effort required by the solver, the choice of this mid-fidelity numerical approach represented the best option to provide parametric data on different types of rotor-rotor interactions and to explore a comprehensive range of space parameters.

2 NUMERICAL MODEL

The propeller model investigated was a three-bladed Varioprop 12C with rotor radius R = 0.15 m. This hobby-grade model propeller was selected to be object of an experimental activity for a thorough validation of numerical investigation. The blade geometry was digitally generated by 3D scanning of the real blade model. The geometrical characteristics of the blade, i.e. twist, dihedral angle, and chord distributions, can be found in [11], while airfoil sections and nacelle geometry will be provided by request to authors. DUST numerical model of propeller blades was built using 40 lifting lines elements for each blade, where tabulated aerodynamic coefficients before stall for blade section airfoils were calculated using XFOIL [12] while Viterna method [13] was used to obtain the post-stall behaviour in the range between $\pm 180^\circ$ of angle of attack. Spinner-nacelle surface was modeled using surface panel elements. The two propellers configurations in tandem and side-by-side studied in the present activity are shown in Fig. 2, where definitions of longitudinal distance between propellers disks planes L_x and lateral distance between propellers shaft axis L_y is illustrated. Numerical simulations were focused on propellers configurations in forward flight, with particular attention on the typical cruise flight velocity of eVTOL urban air mobility vehicles considered in the order of 100 km per hour (i.e., V_∞ = 28 m/s). The rotational speed of both propellers was fixed to 7000 RPM to reproduce the typical full-scale tip Mach number ($M_t = 0.32$) of eVTOL aircraft in cruise [14]. Reynolds number based on propeller disk diameter and on rotational velocity at 70% R was $Re_D = 1.93 \cdot 10^6$, while blade pitch angle at 75% R was fixed to $\theta = 25.5^\circ$ for both propellers. Side-by-side propellers simulations were performed for counter-rotating propellers by changing lateral separation distances in the range between $L_y = 2.05R$ (blade tips distance equal to 0.05R) to $L_y = 4R$. Tandem propellers interaction was investigated considering two co-rotating propellers at two different longitudinal distances between rotor disks, i.e $L_x = 2.5R$ and $L_x = 6R$. Tandem simulations were performed by changing the degree of overlap between rotor disks, i.e. from complete overlap ($L_y = 0$) to a separation distance between propellers shaft axis equal to $L_y = 2R$. Before interacting cases, a preliminary simulation of single propeller was performed to obtain the reference performance and flow field for comparison.

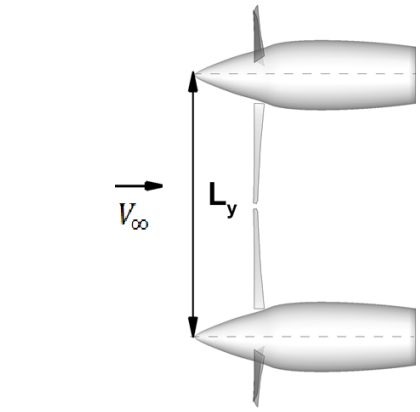

(a) Side-by-side

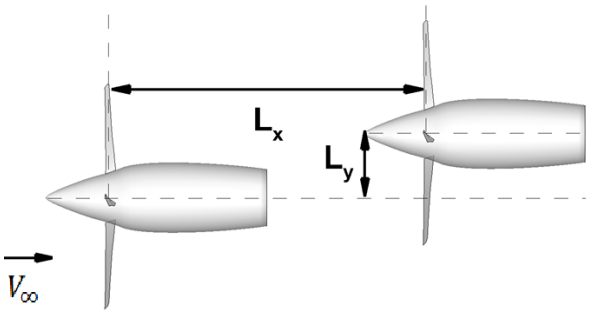

(b) Tandem

Figure 2: Layout of the interacting propellers configurations investigated by numerical simulations.

All simulations were performed for a length of 10 rotors revolutions with a time discretisation of 5° of blade azimuthal angle (ψ)). The computational time of an interacting case was approximately 40 minutes using a workstation with a 18 cores processor.

3 RESULTS AND DISCUSSION

This section presents the most significant results of a selection of numerical simulations performed during this activity for both side-by-side and tandem configurations.

3.1 Side-by-Side Propellers

Figure 3 shows the averaged thrust coefficient C_T and power coefficient C_P computed for the upper propeller in side-by-side configuration normalized with respect to single rotor simulation results. Propeller performance in side-by-side configuration are negligibly affected by aerodynamic interaction as a loss of thrust and power lower than 1% of single propeller values was observed for the lower lateral distance $L_y = 2.05R$. The amount of thrust loss computed

at high advance ratio J = 0.8 is slightly lower than what evaluated in hover by Zhou et al. [2] and by Alvarez et al. [15].

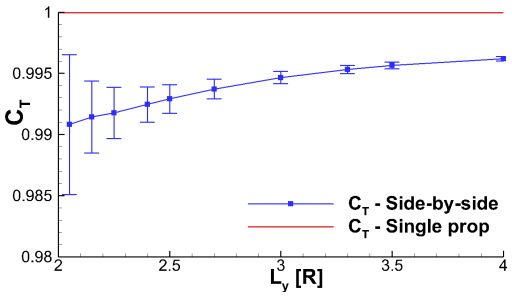

(a)

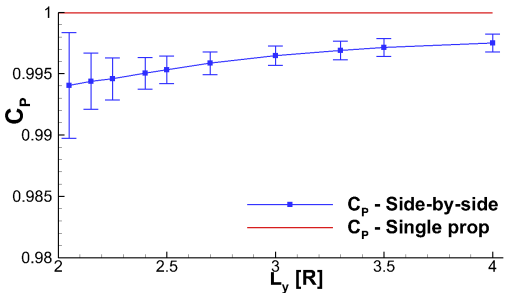

(b)

Figure 3: Side-by-side numerical simulations results, $\theta = 25.5°$, $M_t = 0.32$, $J = 0.8$. Averaged thrust coefficient C_T and power coefficient C_P as function of the lateral distance L_y.

Loads fluctuations amplitude is shown by standard deviation of C_T and C_P plotted as errorbars on the curves depicted in Fig. 3. A high amplitude of loads fluctuations is observed when lateral separation distance between propellers is small as a robust interaction between tip vortices is expected. On the other hand, load fluctuations amplitude decreases as separation distance between propellers increases. A physical analysis of local propeller blades performance for lateral distance $L_y = 2.05R$ can be deduced from Fig. 4, showing the difference of sectional lift coefficient C_l and effective angle of attack α_{eff} experienced by a upper propeller blade in side-by-side configuration with respect to single propeller configuration over last rotor revolution. The polar plot of effective angle of attack variation shows that at $\psi = 0°$, corresponding to azimuthal angle where blade tip-to-tip distance is 0.05R, propeller blade experiences a slight increase of angle of attack at tip region with respect to single propeller condition. Consequently, aerodynamic loads acting on blade tip region increase along the azimuthal range of rotor revolution where side-by-side propeller blades approach each other. Therefore, an increase of sectional C_l with respect to single propeller condition is observed at blade tip region around $\psi = 0°$. On the other hand, a slight decrease of effective angle of attack is experienced by almost all blade sections in azimuthal angle range between $300° < \psi < 330°$ with a consequent decrease of blade loading.

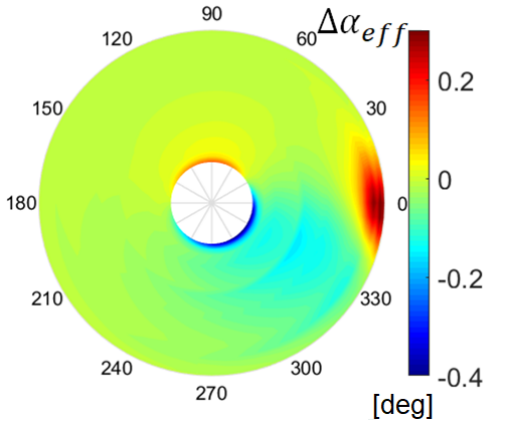

(a)

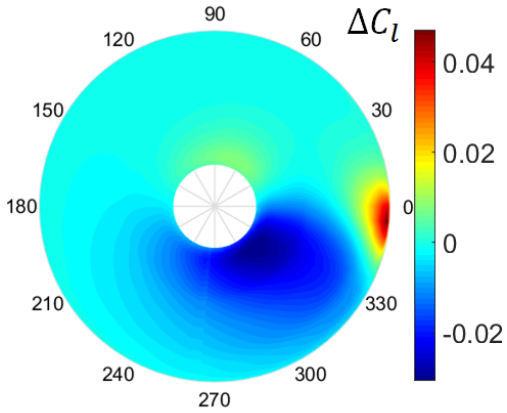

(b)

Figure 4: Variations of effective angle of attack $\Delta\alpha_{eff}$ and sectional lift coefficient ΔC_l on upper propeller in side-by-side configuration at $L_y = 2.05R$ with respect to single propeller configuration [16], $\theta = 25.5°$, $M_t = 0.32$, $J = 0.8$.

For the lower lateral distance between propeller $L_y = 2.05R$, detailed insight regarding flow physics involved in side-by-side aerodynamic interaction is provided by propellers wake comparison with single propeller case. In particular, Fig. 5 shows the contours of average freestream velocity component (u) calculated over last rotor revolution on midspan plane. Flow field representation shows that propellers wakes in side-by-side configuration slightly expands, starting from a distance of 0.5 R downstream the propellers disks before merging at about 3.5 R. This effect produces an increase of the resulting flow speed in this region with respect to single propeller wake. The wake topology observed in cruise flight conditions is similar to what found in the experiments by Zhou et al. [2] for hover conditions, where wakes boundaries merging occurs further upstream. Further details on flow physics that characterises side-by-side interaction are obtained analysing the comparison of the instantaneous in-plane vorticity fields calculated

at $\psi = 0^\circ$ shown in Fig. 6.

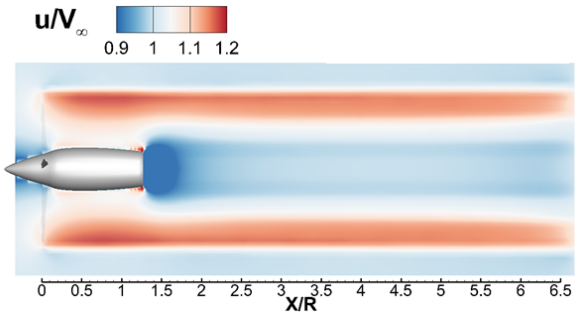

(a) Single propeller

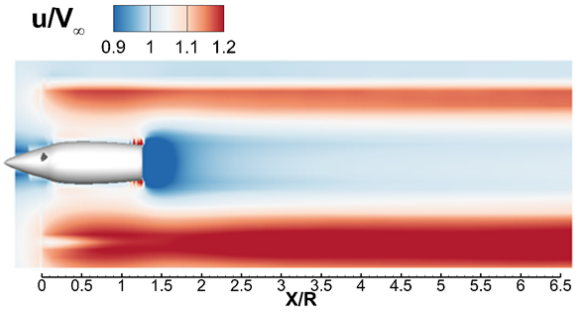

(b) Side-by-side propellers—$L_y = 2.05R$

Figure 5: Comparison of the averaged freestream velocity component computed on midspan plane between single propeller and side-by-side propellers configuration with $L_y = 2.05R$, $\theta = 25.5^\circ$, $M_t = 0.32$, $J = 0.8$.

Single propeller wake representation shows a periodic shed of counter-rotating tip vortices that are dragged downstream by freestream velocity and conserve their relative distance showing a slow rate of dissipation throughout the entire area of investigation. On the other hand, for the side-by-side interaction case, the tip vortices were found to merge starting from $X/R = 0.5R$ downstream the propellers disks and dissipate much faster with respect to single propeller case. Indeed, from $X/R = 1R$ downstream propellers disks, the vortices loose their coherent structures and they are nearly unrecognizable in the wake region between the two propellers.

3.2 Tandem Propellers

Figure 7a shows the thrust coefficient C_T and power coefficient C_P of rear propeller in tandem normalised with respect to single propeller simulations values. The rotor-rotor interaction on rear propeller performance is higher increasing the degree of overlapping between propellers disks, while interactional effects become negligible for lateral separation distance equal to propeller diameter, i.e. $L_y = 2R$. In particular, a decrease of about 45% and 30%, respectively, of thrust and power coefficients is observed with respect to single propeller case when propellers disks are completely overlapped, i.e. $L_y = 0$ with longitudinal distance $L_x = 6R$. At lower longitudinal separation distance between propellers $L_x = 2.5R$ a slight decrease of performance loss, in the order of few percents, is observed for both thrust and power coefficients.

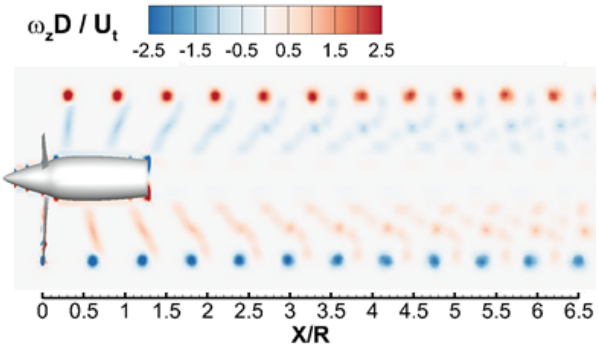

(a) Single propeller

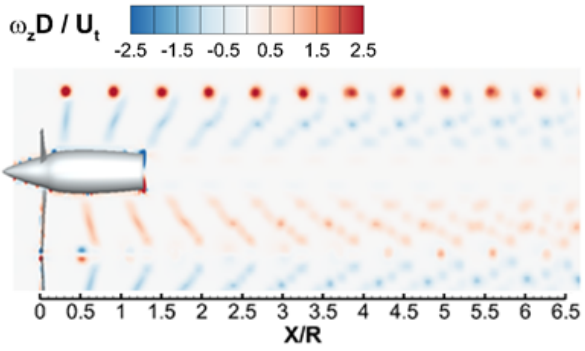

(b) Side-by-side propellers—$L_y = 2.05R$

Figure 6: Comparison of the in-plane vorticity component ω_z computed on midspan plane between the single propeller and side-by-side propellers configuration with $L_y = 2.05R$ at $\psi = 0^\circ$, $\theta = 25.5^\circ$, $M_t = 0.32$, $J = 0.8$.

The amplitude of loads fluctuations is depicted as errorbars on the C_T and C_P curves, as done for the side-by-side propellers case. A higher standard deviation of loads is observed when the lateral separation distance between propellers is $L_y = 1R$. Loads fluctuations level decreases by increasing the degree of overlapping between propellers disks and become negligible when propellers disks are completely overlapped. Moreover, for lateral separation distances higher than $L_y = 1R$, thrust and power coefficients of rear propeller in tandem approach the single propeller values, while loads fluctuations amplitude decreases.

A physical analysis of local propeller blades performance for lateral distances $L_y = 0, 0.5R, 1R$ can be deduced from Fig. 8, showing the differences with respect to single propeller configuration of axial velocity u_a, tangential velocity u_t, effective angle of attack α_{eff}, and sectional lift coefficient C_l of a rear propeller blade in tandem configuration at $L_x = 6R$.

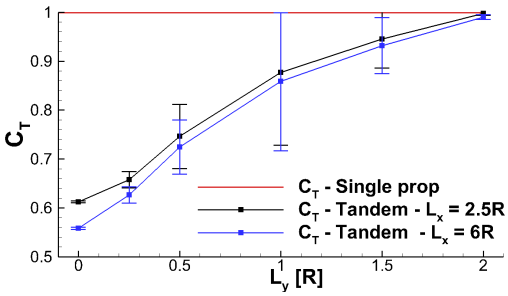

(a)

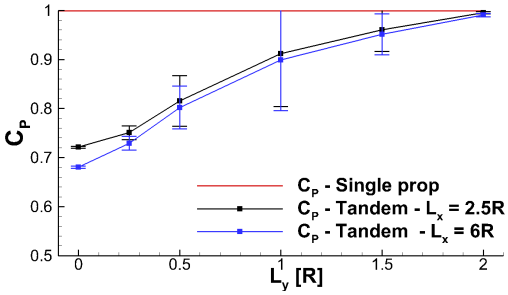

(b)

Figure 7: Tandem numerical simulations results, $\theta = 25.5°$, $M_t = 0.32$, $J = 0.8$. Averaged thrust coefficient C_T and power coefficient C_P of the rear propeller as function of the lateral distance L_y.

When propeller disks are completely overlapped ($L_y = 0$) the rear propeller blade experiences an increase of axial velocity due to the ingestion of front propeller slipstream, that is particularly apparent on the outer spanwise blade region. Moreover, rear propeller blade experienced also a slight negative variation of tangential velocity due to front propeller slipstream interaction. Consequently, a reduction of the local effective angle of attack and of sectional lift is experienced by rear propeller blade on a large portion along span. This physical effect reflects the large loss of average thrust calculated on rear propeller in tandem. Moreover, the axial-symmetrical behaviour of ΔC_l reflects the negligible amount of loads fluctuation for this tandem configuration. When propeller disks are partially overlapped, i.e. $L_y = 0.5R$, the polar plots shown in Fig. 8 loose their axial-symmetrical behaviour. In particular, axial velocity component is consistently increased in the azimuthal region between $\psi = 190°$ and $\psi = 230°$ due to the local acceleration of front propeller slipstream provided by the cambered shape of nacelle-spinner. On the other hand, the interaction with front propeller wake provides negligible modifications on tangential velocity of rear propeller blade. The combination of axial and tangential velocity variations provides a reduction of effective angle of attack experienced by rear blade sections in azimuthal angle ranges $190° < \psi < 230°$ and $330° < \psi < 360°$, with a consequent large negative variation of rear blade sectional lift distributions. This behaviour reflects the remarkable amount of loads fluctuation amplitude calculated for this tandem configuration. Decreasing the degree of overlapping between propellers disks, i.e. $L_y = 1R$, the front propeller slipstream interaction provides a concentrated increase of axial velocity component behaviour on rear propeller blade in the azimuthal range between $\psi = 180°$ and $\psi = 360°$. This effect is due to the local acceleration of front propeller slipstream in this area provided by the nacelle-spinner curvature. Wake interactions also provides a large increase of tangential velocity experienced by rear propeller blade in the same azimuthal range. Consequently, a remarkable decrease of effective angle of attack and sectional lift is experienced by rear propeller blade sections in azimuthal ranges $210° < \psi < 240°$ and $300° < \psi < 330°$. In particular, sectional lift behaviour variation reflects the larger amplitude of loads fluctuations observed for this tandem configuration. Detailed insight about flow physics involved in tandem propellers aerodynamic interaction is provided by the analysis of averaged propellers wakes flow fields for configurations with lateral distances $L_y = 0, 0.5R, 1R$, see Fig. 9. When propeller disks are completely overlapped, i.e. $L_y = 0$, the rear propeller wake is quite faster at tip region of propeller disk with respect to front propeller one due to a combination of accelerated flow regions passing through the outer regions of propeller disks. Decreasing the degree of overlapping between propeller disks, i.e. $L_y = 0.5$, an asymmetrical behaviour of rear propeller wake with respect to longitudinal axis is observed due to front propeller slipstream interaction. Indeed, the rear propeller wake lower flow region is accelerated by the effect of front propeller slipstream, while the upper region of front propeller slipstream is dragged upward and locally accelerated by the cambered shape of nacelle-spinner surface. A similar asymmetrical behaviour of rear propeller wake is observed for $L_y = 1R$. In particular, due to the higher degree of overlapping between propeller disks, the front propeller slipstream upper flow region is dragged downward and locally accelerated by the presence of rear propeller nacelle with a consequent increase of accelerated flow area that can be observed in the lower region of rear propeller wake. More details on tandem aerodynamic interaction physics are provided by the comparison of in-plane vorticity calculated from instantaneous flow field at $\psi = 0°$ shown in Fig. 10. Due to synchronised co-rotating propellers blades, the tip vortices shed by front propeller blades interact with rear propeller ones providing co-rotating vortical structures characterised by higher vorticity and larger core downstream rear propeller disk. At lateral distance between propellers $L_y = 0.5R$ the upper region of front propeller wake diverges upward due to the presence of rear propeller nacelle. Consequently, the vortices released by front propeller blades are dragged toward rear propeller ones in the upper wake flow region past propeller disk. This interaction provides a pairing of co-rotating vortices and the shear layer winding into a series of counter-rotating vortices. At lateral distance between propellers $L_y = 1R$, the tip vortices shed by front propeller blades dissipate impinging on rear propeller nacelle nose.

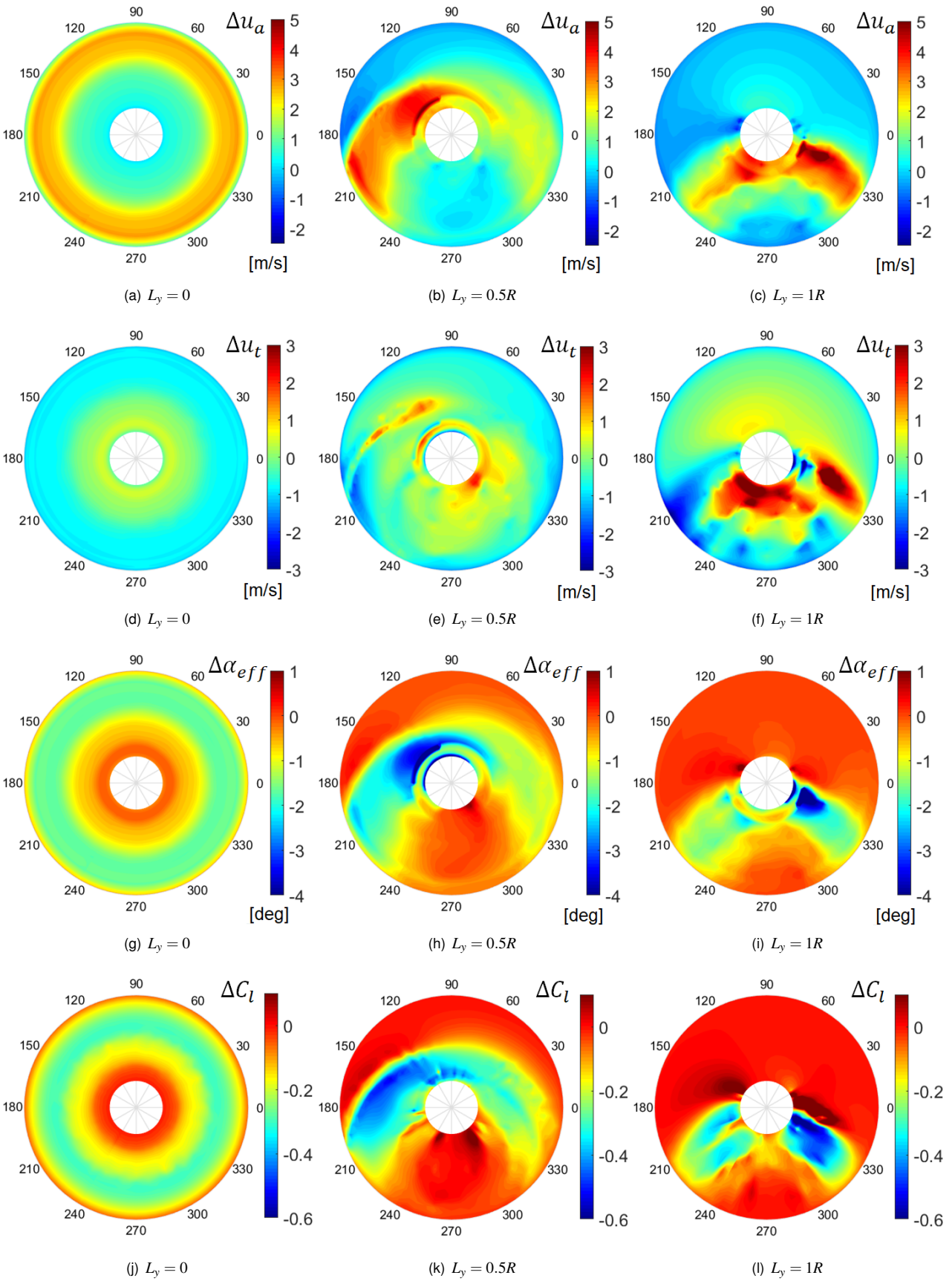

(a) $L_y = 0$ (b) $L_y = 0.5R$ (c) $L_y = 1R$

(d) $L_y = 0$ (e) $L_y = 0.5R$ (f) $L_y = 1R$

(g) $L_y = 0$ (h) $L_y = 0.5R$ (i) $L_y = 1R$

(j) $L_y = 0$ (k) $L_y = 0.5R$ (l) $L_y = 1R$

Figure 8: Variations of axial velocity Δu_a, tangential velocity Δu_t, effective angle of attack $\Delta \alpha_{eff}$ and sectional lift coefficient ΔC_l on rear propeller blade in tandem configuration at $L_x = 6R$ with respect to single propeller configuration for the last rotor revolution [16], $\theta = 25.5°$, $M_t = 0.32$, $J = 0.8$.

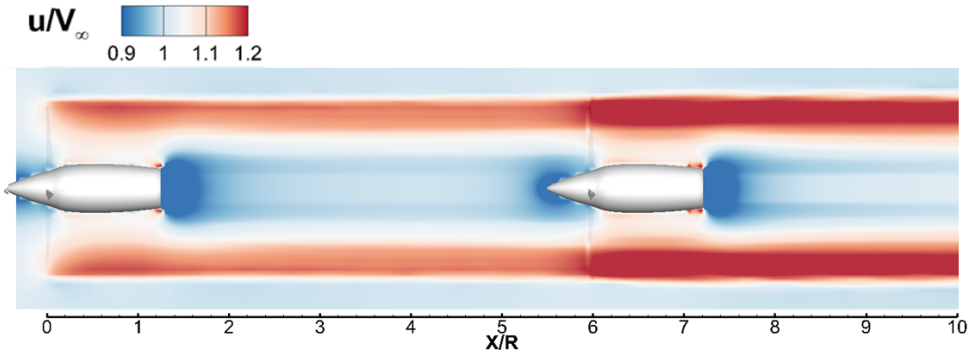

(a) $L_y = 0$

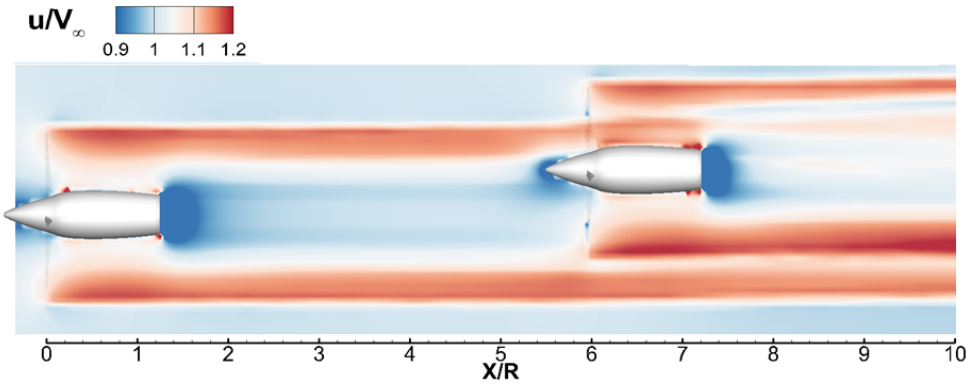

(b) $L_y = 0.5R$

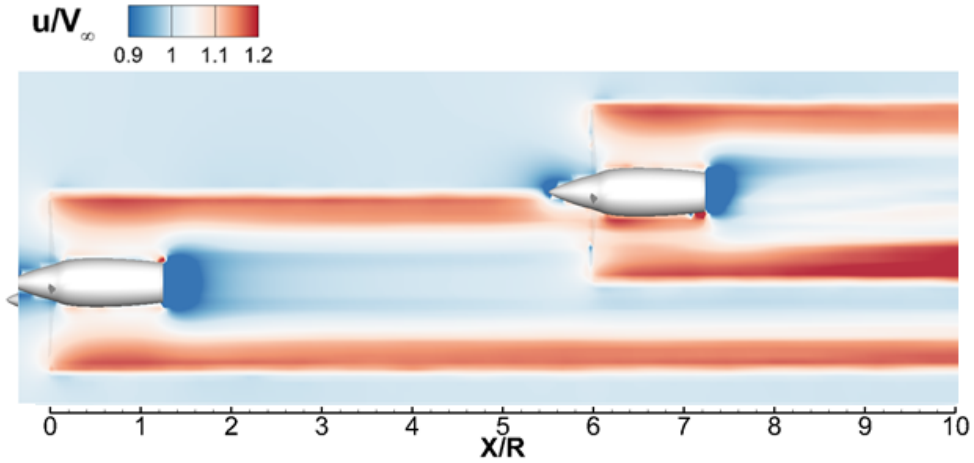

(c) $L_y = 1R$

Figure 9: Comparison of averaged freestream velocity component computed on midspan plane for tandem propellers configurations with $L_x = 6R$, $\theta = 25.5°$, $M_t = 0.32$, $J = 0.8$.

4 CONCLUSIONS

A mid-fidelity numerical approach was used to investigate rotor-rotor aerodynamic interactions typical of eVTOL aircraft architectures. A systematic series of numerical simulations were performed with DUST on two propellers both in side-side and tandem configurations in cruise flight condition. Side-by-side simulations results showed a slight reduction of average propeller thrust with respect to single propeller configuration. On the other hand, a high amplitude of load fluctuations was observed at low separation distance between propellers that could provide a drawback for aeroacoustic issues. Tandem simulations results analysis showed a remarkable decrease of rear propeller performance due to front propeller slipstream aerodynamic interaction. The local blade aerodynamic loads analysis shows that a partial degree of overlapping between propellers disks provides a lower effect on rear propeller blades loading but a larger amplitude of loads fluctuation along a rotor revolution with respect to co-axial configuration.

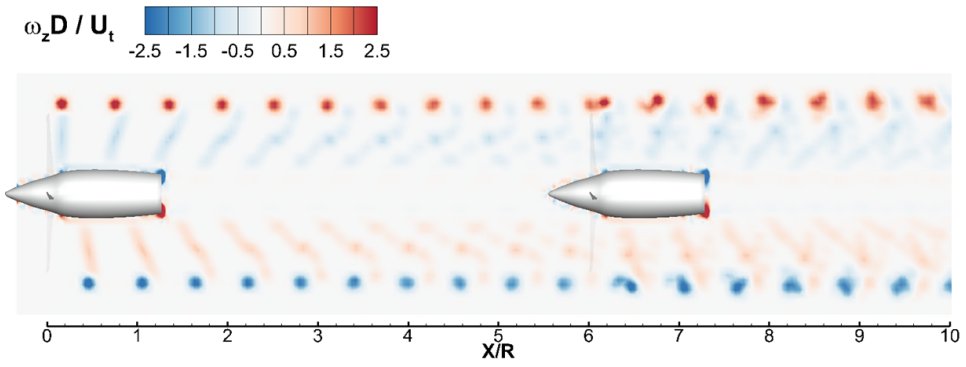

(a) $L_y = 0$

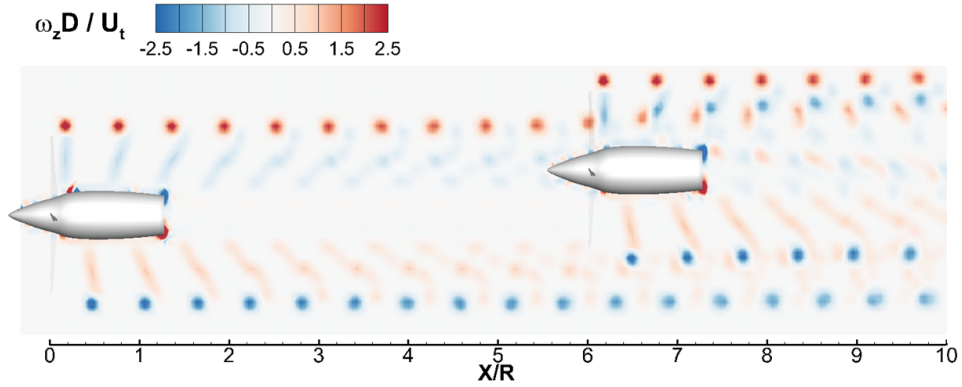

(b) $L_y = 0.5R$

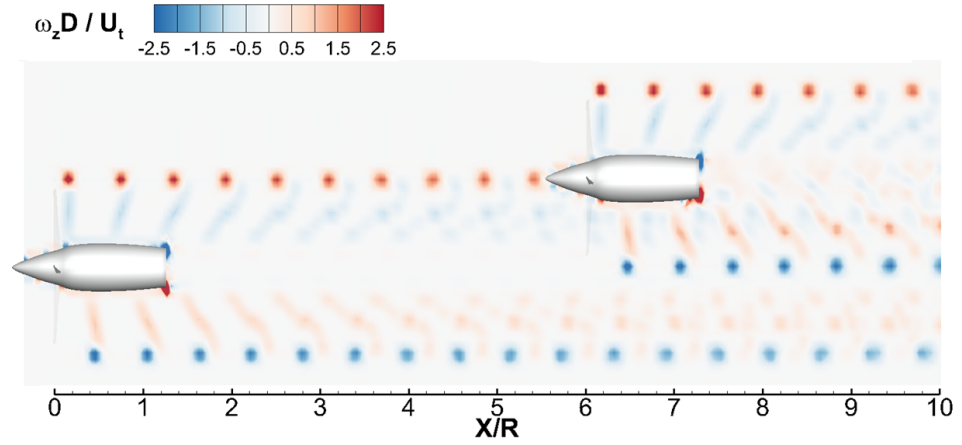

(c) $L_y = 1R$

Figure 10: Comparison of the in-plane vorticity component ω_z computed on midspan plane for tandem propellers configurations with $L_x = 6R$ at $\psi = 0°$, $\theta = 25.5°$, $M_t = 0.32$, $J = 0.8$.

Flow fields analysis illustrated flow physics interaction between front propeller slipstream and rear propeller wake, showing, in particular, the tip vortices pairing that occurs with co-axial propellers disks or with a low degree of overlapping between them. Generally, the present activity produced a comprehensive numerical database for eVTOL research community to be used to drive the design of new unconventional aircraft configurations. A thorough validation of the numerical simulations will be performed in the next future by means of comparison with experimental data provided by a wind tunnel campaign already performed at Politecnico di Milano.

Copyright Statement

REFERENCES

[1] Nicholas Polaczyk, Enzo Trombino, Peng Wei, and Mihaela Mitici. A review of current technology and research in urban on-demand air mobility applications. In *Proceedings of the Vertical Flight Society's 6th Annual Electric VTOL Symposium*, Mesa, AZ, USA, 29–31 January 2019.

[2] W Zhou, Z Ning, H Li, and H Hu. An experimental investigation on rotor-to-rotor interactions of small uav propellers. In *Proceedings of the 35th AIAA Applied Aerodynamics Conference*, Denver, USA, 5–8 June 2017.

[3] D Shukla and N Komerath. Multirotor drone aerodynamic interaction investigation. *Drones*, 2(4):1–13, 2018.

[4] D Shukla, N Hiremath, and Komerath NM. Low reynolds number aerodynamics study on coaxial and quad-rotor. In *Proceedings of the 53th AIAA Aviation Forum*, Atlanta, GA, USA, 25–27 June 2018.

[5] M Brazinskas, SD Prior, and JP Scanlan. An empirical study of overlapping rotor interference for a small unmanned aircraft propulsion system. *aerospace*, 3(32), 2016.

[6] Davide Montagnani, Matteo Tugnoli, Federico Fonte, Alex Zanotti, Giovanni Droandi, and Monica Syal. Mid-fidelity analysis of unsteady interactional aerodynamics of complex vtol configurations. In *45th European Rotorcraft Forum, Sept. 2019, Warsaw, Poland*, 2019.

[7] Matteo Tugnoli, Davide Montagnani, Monica Syal, Giovanni Droandi, and Alex Zanotti. Mid-fidelity approach to aerodynamic simulations of unconventional vtol aircraft configurations. *Aerospace Science and Technology*, 115:106804, 2021.

[8] Georges-Henri Cottet, Petros D Koumoutsakos, D Petros, et al. *Vortex methods: theory and practice*. Cambridge University Press, 2000.

[9] Alex Zanotti, Alberto Savino, Michele Palazzi, Matteo Tugnoli, and Vincenzo Muscarello. Assessment of a mid-fidelity numerical approach for the investigation of tiltrotor aerodynamics. *Applied Sciences*, 11(8):3385, 2021.

[10] Giovanni Droandi, Monica Syal, and Geoffrey Bower. Analysis of the interactional aerodynamics of the vahana evtol using a medium fidelity open source tool. In *Proceedings of the VFS Aeromechanics for Advanced Vertical Flight Technical Meeting*, San Jose, CA, USA, January 21-23 2020. AHS International.

[11] R. Piccinini. Rotor-rotor aerodynamic interactions for evtol aircraft configurations. Master's thesis, Politecnico di Milano, 2020.

[12] Mark Drela. Xfoil: An analysis and design system for low reynolds number airfoils. In Thomas J. Mueller, editor, *Low Reynolds Number Aerodynamics*, pages 1–12, Berlin, Heidelberg, 1989. Springer Berlin Heidelberg.

[13] L A Viterna and D C Janetzke. Theoretical and experimental power from large horizontal-axis wind turbines. Technical report, Washington Procurement Operations Office, Washington, DC (United States), Setptember 1982.

[14] Giovanni Droandi, Monica Syal, and Geoffrey Bower. Tiltwing multi-rotor aerodynamic modeling in hover, transition and cruise flight conditions. In *Proceedings of the 74th Annual Forum*, Phoenix, May 2018. AHS International.

[15] EJ Alvarez and A Ning. Modeling multirotor aerodynamic interactions through the vortex particle method. In *Proceedings of the 54th AIAA Aviation Forum*, Dallas, TX, USA, 17–19 June 2019.

[16] Riccardo Piccinini, Matteo Tugnoli, and Alex Zanotti. Numerical investigation of the rotor-rotoraerodynamic interaction for evtol aircraftconfigurations. *Energies*, 13(22):1–28, 2020.